



Second-grade fluid with carbon nanotubes flowing over an elongated curve surface possessing thermal radiation and internal heat generation effects

Zain Ul Abideen¹ · Rai Sajjad Saif² · Taseer Muhammad³

Received: 18 June 2023 / Accepted: 13 November 2023 / Published online: 2 February 2024
© Akadémiai Kiadó, Budapest, Hungary 2024

Abstract

The goal of the current research is to analyze heat transmission of radiative nanofluid with reference to boundary layer nature. Carbon nanotube's (CNT's) reliant liquid is being tested, and it flows on top of a curved extending surface. To scrutinize thermal transmission through the flow additional impacts of thermal radiation as well as internal heat generation have been incorporated. Dual nature of CNTs, that is, single-walled CNTs (SWCNTs) and multi-walled CNTs (MWCNTs) have been employed in conjunction with slurry mixture (base fluid) for the formulation of nanofluid. Second-grade fluid model is engaged in order to capture the rheological properties of slurry mixtures (base fluid). To acquire the numerical solution of designed mathematical model, NDSolve approach is engaged using software Mathematica. Various parameters occurring in governing equations makes an impact on focused physical quantities. Graphs have been employed to capture these impacts for both SWCNTs and MWCNTs. In like manner, the impact of numerous factors on skin friction coefficient as well as Nusselt number have been examined using numerical charts. An increment in dimensionless curvature parameter causes a decline in fluid's velocity profile as well as temperature profile. However, both fluid's velocity and temperature get enhanced as an upsurge in solid volume fraction of carbon nanotubes, radiation parameter and heat generation parameter.

Keywords Second-grade nanofluid · Internal heat generation · Thermal radiation · Carbon nanotubes (CNTs: SWCNTs-MWCNTs) · Curved stretching surface · Numerical solution

List of symbols

(\dot{u}, \dot{v})	Velocity components (ms^{-1})	α_{nf}	Thermal diffusivity of nanofluid ($\text{m}^2 \text{s}^{-1}$)
\dot{R}_c^*	Radius of curvature (m)	\dot{a}_R	Roseland mean approximation coefficient
a	Stretching constant (s^{-1})	ρ_f	Fluid density (kg m^{-3})
$\dot{\alpha}_1$	Second-grade fluid parameter	ρ_{CNT}	Carbon nanotubes density (kg m^{-3})
$(\rho C_p)_{\text{nf}}$	Nanofluid heat capacity	ν_f	Base fluid kinematic viscosity ($\text{m}^2 \text{s}^{-1}$)
μ_f	Base fluid dynamic viscosity (kg ms^{-1})	ζ	Similarity variable
k_f	Base fluid thermal conductivity $\text{W m}^{-1} \text{K}^{-1}$	κ	Dimensionless radius of curvature
C_p	Specific heat $\text{J kg}^{-1} \text{K}^{-1}$	l	Characteristic length (m)
k_{CNT}	Thermal conductivity of CNTs $\text{W m}^{-1} \text{K}^{-1}$	A	Reference temperature (K)
		τ_{is}	Wall shear stress (Pa)
		Re_ξ	Local Reynolds number
		\dot{r}, \dot{s}	Coordinate axes (m)
		P	Pressure (Pa)
		$\dot{\gamma}$	Volumetric heat generation (J)
		\dot{q}_r	Radiative heat flux (J)
		ϕ	Nanoparticles concentration
		μ_{nf}	Nanofluid dynamic viscosity (kg ms^{-1})
		k_{nf}	Nanofluid thermal conductivity $\text{W m}^{-1} \text{K}^{-1}$
		\dot{T}	Temperature (K)
		\dot{T}_w	Surface temperature (K)
		\dot{T}_∞	Free stream temperature (K)

✉ Rai Sajjad Saif
rai.sajjad@seecs.nust.edu.pk; raiqau@gmail.com

¹ School of Natural Sciences (SNS), National University of Sciences and Technology (NUST), Islamabad, Pakistan

² Department of Humanities and Sciences, School of Electrical Engineering and Computer Science (SEecs), National University of Sciences and Technology (NUST), Islamabad, Pakistan

³ Department of Mathematics, College of Sciences, King Khalid University, Abha 61413, Saudi Arabia

δ^*	Stefan–Boltzmann constant ($\text{W m}^{-2} \text{K}^{-4}$)
R_D	Radiation parameter
Pr	Prandtl number
ν_{nf}	Nanofluid kinematic viscosity ($\text{m}^2 \text{s}^{-1}$)
λ_1	Heat generation parameter
θ	Dimensionless temperature
f'	Dimensionless velocities
\dot{q}_w	Wall heat flux (W m^{-2})
C_f	Skin friction coefficient
Nu_s	Local Nusselt number

Introduction

Nanofluids are a type of fluid that have been infused with tiny nanoparticles. These nanoparticles can be made up of a variety of materials, including metals, oxides and other materials. When these nanoparticles are mixed into a fluid, they can dramatically change its properties. Nanofluids have been shown to have enhanced thermal conductivity, improved lubrication and increased stability. They also have the potential to improve a wide range of medical and industrial processes from cooling systems to energy production. Nanofluids can be used in medical imaging, drug delivery, tissue engineering and cancer treatment. Choi [1] was the explorer who laid the groundwork for the evolution of nanofluids as a new category of thermal transmitted fluids. He proposed the idea that adding small amounts of nanoparticles to a fluid could dramatically enhance its thermal conductivity. Soon after this, Kim et al. [2] investigated the convective instability and heat transmission properties of nanofluids. Buongiorno [3] documented a study to explain the convective heat transmission in nanofluids. Tiwari and Das [4] examined the heat transfer performance of a square cavity filled with nanofluid under differentially

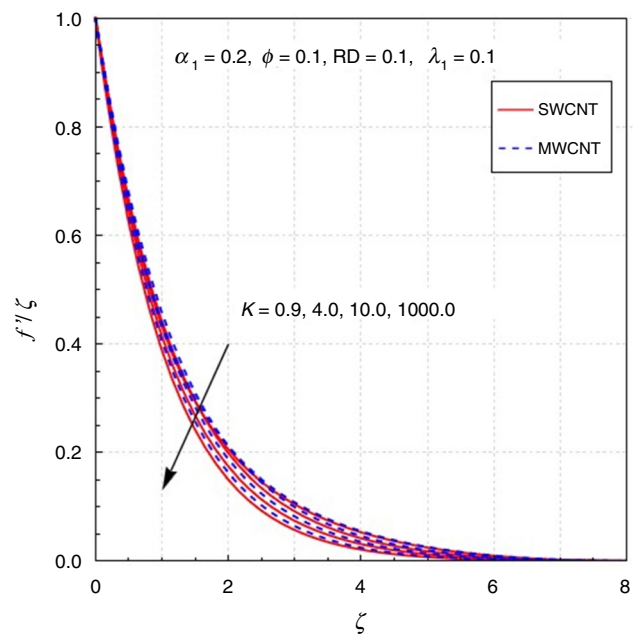
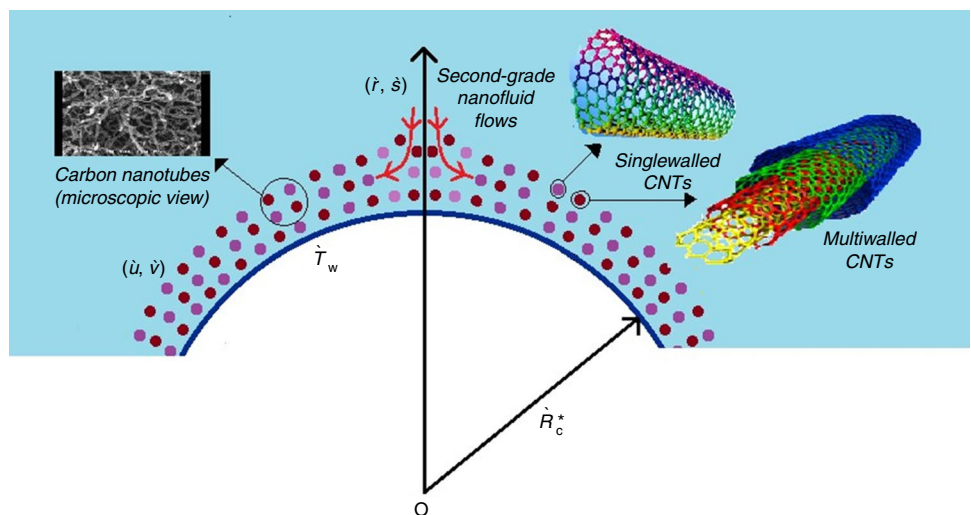


Fig. 2 Action of (κ) over $f'(\zeta)$

heated conditions. The study also investigates the influence of the lid-driven motion on the heat transfer performance of the nanofluid. Buongiorno’s work [3] was extended by Khan and Pop [5] in regard to boundary layer nano-liquid flow over a stretchable sheet. The examination explored the effects of various parameters such as the stretching rate, nanoparticle volume fraction, thermal conductivity and heat transfer characteristics of the nanofluid. The heat and mass transmission phenomenon of nanofluid flow past a vertical plate under natural convection conditions were elaborated by Kuznetsov et al. [6]. Cu–H₂O-based nanofluid was evaluated and documented by Raza et al. [7], by taking into account the impact of Brownian motion and thermophoresis, which

Fig. 1 Geometrical perspective of problem



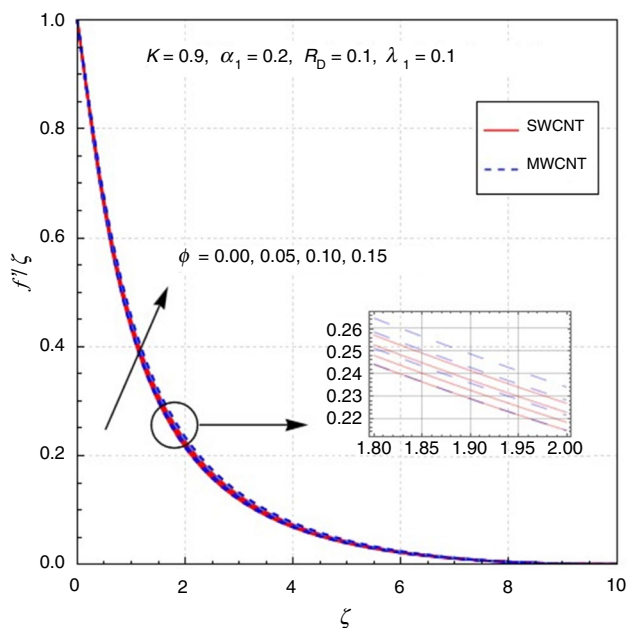


Fig. 3 Action of (ϕ) over $f'(\zeta)$

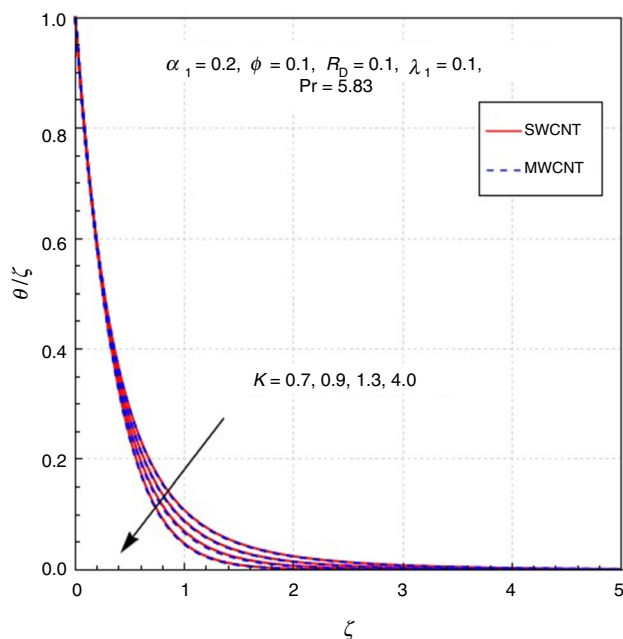


Fig. 5 Action of (κ) over $\theta(\zeta)$

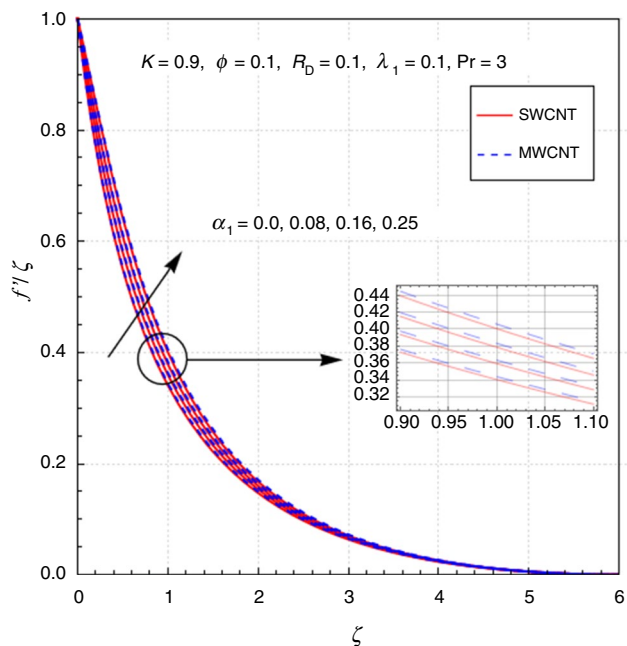


Fig. 4 Action of (α_1) over $f'(\zeta)$

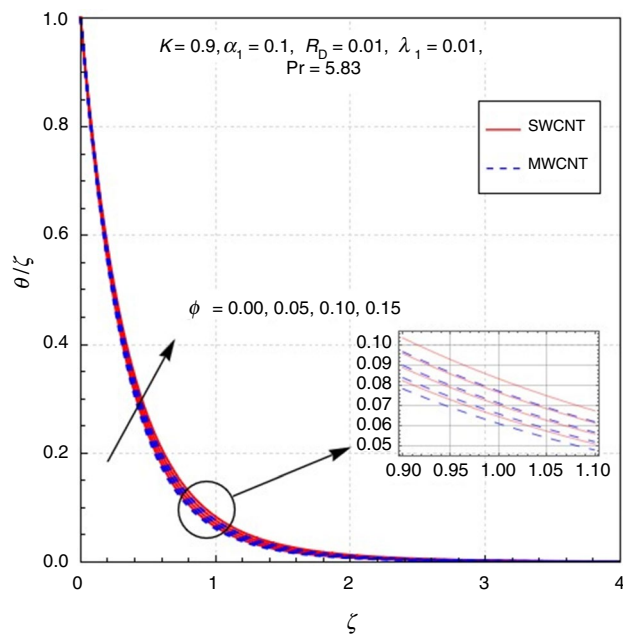


Fig. 6 Action of (ϕ) over $\theta(\zeta)$

are two unique properties of nanofluids. Further literature can be seen [8–10].

Carbon nanotubes (both single and multiple-walled) are one of the most fascinating and promising materials of our time. These incredibly small tubes are made up of carbon atoms, arranged in a unique way that creates a strong, flexible and highly conductive structure. They are so small that

they are measured in nanometers or billionths of a meter. Carbon nanotubes have the strength to revolutionize a broader aspect of industries from electronics to medicine to energy. They are already being used in everything from super-strong materials to ultrafast computer chips, and scientists are constantly discovering new ways to harness their unique properties. Maxwell [11] conducted a formal

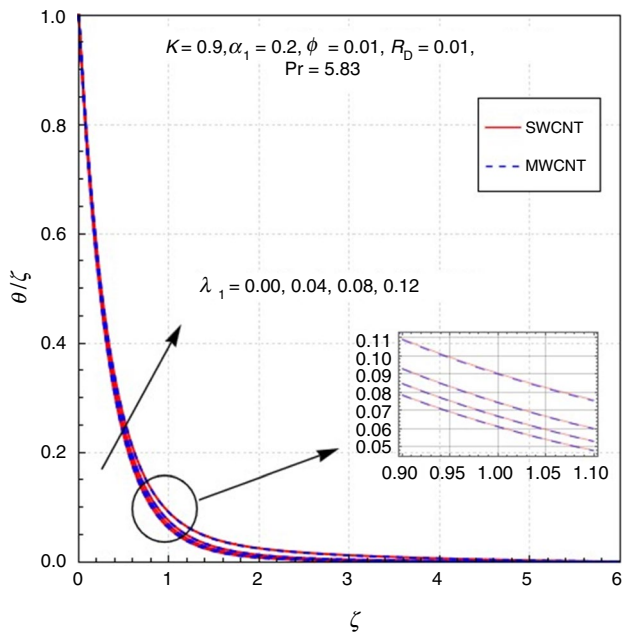


Fig. 7 Action of (λ_1) over $\theta(\zeta)$

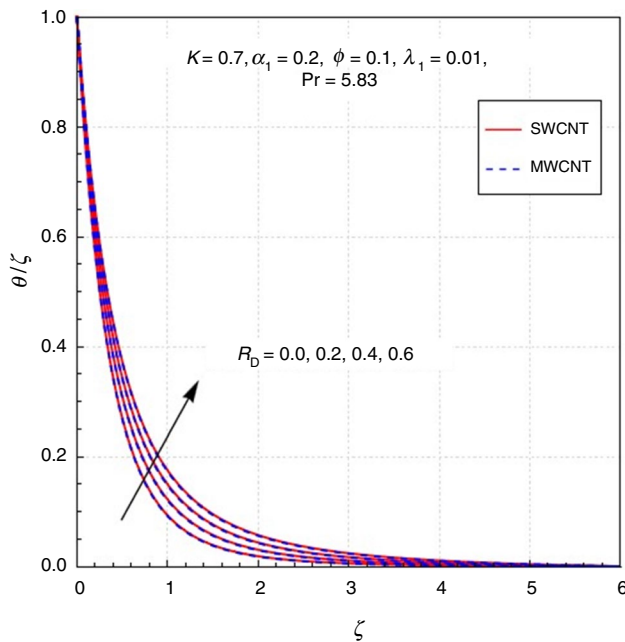


Fig. 8 Action of (R_D) over $\theta(\zeta)$

investigation on carbon nanotubes, exploring their effects on electricity and magnetism. Later on, Xue [12] developed a model to predict the thermal conductivity of CNT-based composites. The model takes into account the microstructure of the composites, including the orientation, length and concentration of the CNTs as well as the thermal conductivity of the surrounding matrix material. Khan et al. [13]

investigated the dynamics of Stoke’s first problem for CNTs suspended nanofluids in the presence of slip boundary condition. The results of the study show that the inclusion of CNTs enhances the heat transmission rate and the skin friction coefficient, while slip boundary condition has a prominent impact on the fluid flow and heat transfer performance of the nanofluid. Hayat et al. [14] investigated the radiation effects for nanofluid flow over a rotating disk in the presence of carbon nanotubes (CNTs) and partial slip. Wakif et al. [15] performed a semi-analytical analysis of electrothermo-hydrodynamic stability in dielectric nanofluids using Buongiorno’s mathematical model. A mathematical model to analyze the behavior of CNT-based nanomaterial flow in the presence of two coaxially circulating disks was unveiled by Khan et al. [16]. The results of the study show that the existence of CNTs enhances the heat transmission rate and reduces the occurrence of entropy, while affecting the flow and temperature fields of the nanomaterial. Acharya et al. [17] scrutinized the mixed convective flow of carbon nanotubes (CNTs) over a convectively heated curved surface. Due to the prominent applications of carbon nanotubes, many researchers tried to harness the properties of CNTs [18–22].

Nowadays scrutinization of non-Newtonian fluids has become the central hotspot for engineers and scientists owing to its bright and encouraging applications in industry. Non-Newtonian fluids are fluids which disobey law of viscosity unveiled by Newton. Salient utilization of non-Newtonian liquids incorporates; drag reducing agents (heavy oils and greases), printing technology, biological systems and strategies, food processing, fluorescent lamps, electric devices and many others. One of many proposed non-Newtonian

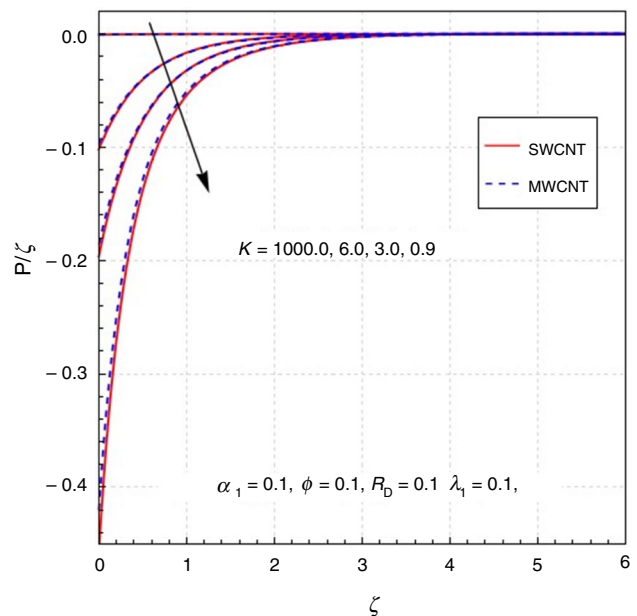


Fig. 9 Action of (κ) over $P(\zeta)$

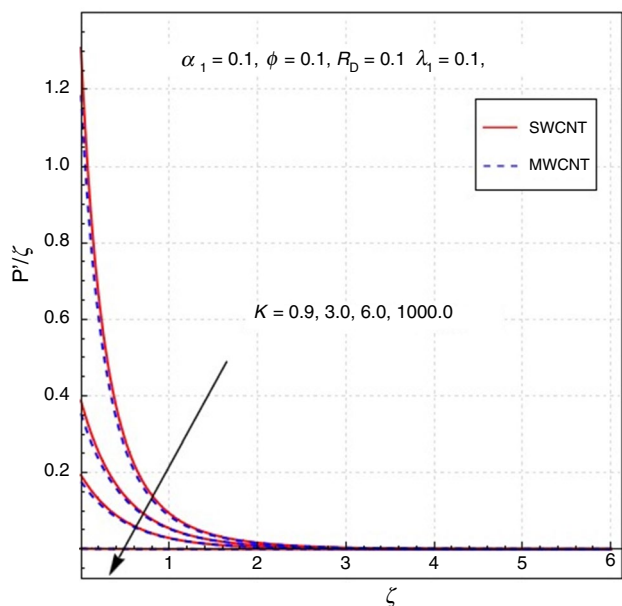


Fig. 10 Action of (κ) over $P'(\zeta)$

liquids is second-grade fluid, which possesses stress tensor relationship with dual derivatives. In recent times, Hayat and Sajid [23] amplified second-grade axisymmetric fluid flow past an elastic sheet. Saif et al. [24] given thought to a stagnation point stream of a second-grade nano-material in the vicinity of nonlinear extending surface with a fluctuating thickness. Abderrahim [25] documented a numerical procedure in order to simulate steady MHD flows of radiative Casson fluids over a horizontal stretching sheet. Hayat et al. [26] given an explanation of second-grade fluid flow across a porous surface. Radiative stream of a second-grade nanofluid overtop an extending surface was illustrated by Jamshed et al. [27]. The Stefan blowing impact was incorporated by Gowda et al. [28] to investigate the second-grade fluid flow overtop a curved elastic surface. Further literature can be found at [29–32].

The study of fluid flow over a stretchable boundary is essential in the manufacturing of polymer films, sheets and fibers. Stretching of polymer materials is a critical step in the formation of these materials and proper understanding of the boundary layer flow is essential for achieving the desired properties. Moreover in the production of textiles, boundary layer flow over a stretching surface plays a crucial role in the

Fig. 11 Action of (κ) over (Cf)

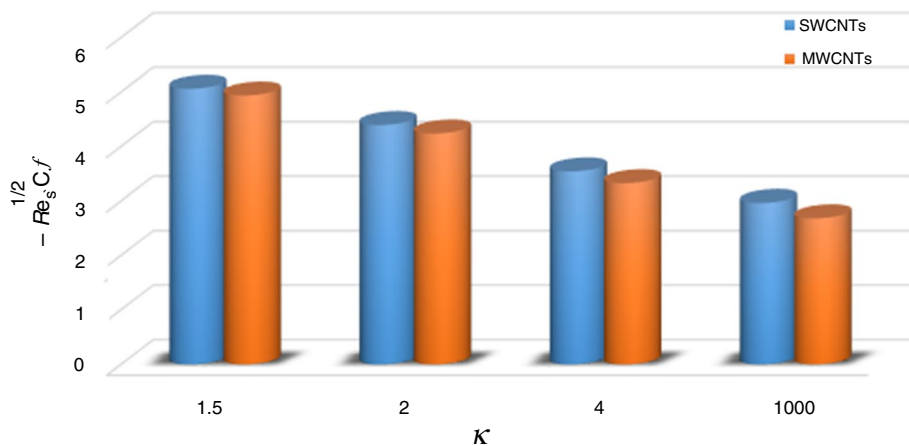
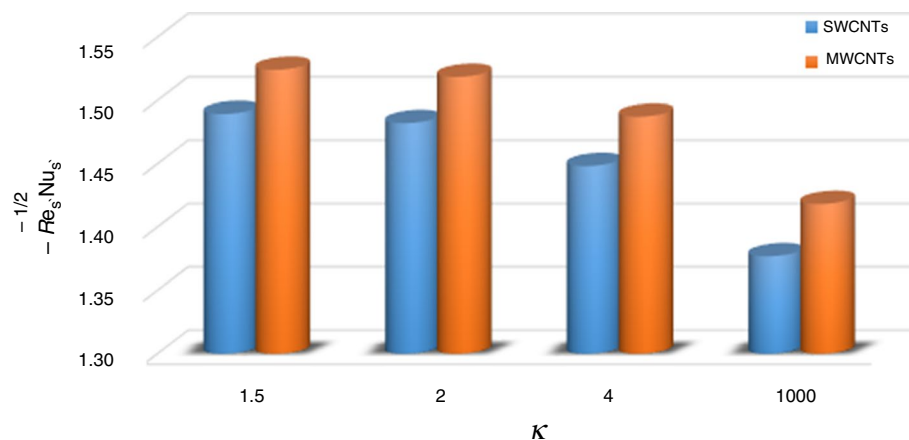


Fig. 12 Action of (κ) over (Nu)



spinning and weaving of fibers. Aerodynamics, bio-inspired robotics, wind and water turbines are some crucial practical applications of boundary layer flow across a flexible surface. Sakiadis [33] initiated the investigations of streams in regard with boundary layer description across a stretchable surface and unveiled its numerical findings. The 2-D laminar flow of viscous fluid across a stretchable sheet was investigated by Crane [34]. Most of the previous studies incorporated boundary layer flow due to stretching surface, either linear or nonlinear; however, scrutinization of fluid flows through curved extending surfaces has not been studied much. Sajid et al. [35] were the pioneers who initiated the study of fluid flow in regard with boundary layer description across a curved elongating surface. Hayat et al. [36] illustrated the effects of Darcy–Forchheimer flow, Cattaneo–Christov heat flux as well as heterogeneous-homogeneous reactions on the behavior of viscous fluid flow over a curved stretching surface. Hayat et al. [37] unveiled a numerical model to analyze the influences of convective heat and mass transfer via nonlinear curved stretching sheet. Sugunamma et al. [38] documented the impact of frictional heated radiative ferrofluid flow over a slandering stretchable surface. Further work can be seen at [39–42].

We conducted this investigation because CNTs are widely used in the engineering and healthcare sectors. Over a curved stretched sheet, we investigated the heat transfer through a radiative flow of a boundary layer description and internal heat generation of a second-grade nanofluid made of carbon nanotubes (SWCNTs and MWCNTs). In-depth literary analysis revealed that a combination of such effects had never before been investigated. As a result, the inquiry is divided into several sections. Following a review of the literature, the first section elaborates the mathematical formulation, while the second section includes the mathematical solution obtained numerically by deploying NDSolve technique using software Mathematica along with significant discoveries via graphical representation. The final portion is set up to draw conclusions from the entire investigation.

Mathematical analysis

The flow under inspection is 2D-steady incompressible flow overtop a curved extending sheet at $\dot{r} = \dot{R}_c^*$. Geometrical vision of problem is described by Fig. 1. Curvilinear coordinates have been engaged to model the governing equations. Nanofluid being studied is composed by introducing nano-sized particles of carbon nanotubes (SWCNTs and MWCNTs) to second-grade fluid (base fluid). Moreover, effects of internal heat generation and thermal radiation have also been utilized to inspect the process of thermal transmission. The

curved sheet is being stretched linearly in \dot{s} direction with velocity $\dot{u} = a\dot{s}$, where $a > 0$ is the stretching constant. The free stream temperature and sheet’s temperature are represented as \dot{T}_∞ and \dot{T}_w , respectively.

The second-grade fluid possess an extra stress tensor [27] defined as

$$\boldsymbol{\tau} = -p\mathbf{I} + \dot{\mu}\mathbf{A}_1 + \dot{\alpha}_1\mathbf{A}_2 + \dot{\alpha}_2\mathbf{A}_1^2, \tag{1}$$

where p denotes pressure, \mathbf{I} indicates identity tensor, $\dot{\mu}$ is dynamic viscosity, $\alpha_j(j = 1, 2)$ are second-grade material constants and the first two Rivlin–Ericksen tensors \mathbf{A}_1 and \mathbf{A}_2 are described as

$$\left. \begin{aligned} \mathbf{A}_1 &= (\text{grad}\mathbf{V})^t + (\text{grad}\mathbf{V}), \\ \mathbf{A}_2 &= \mathbf{A}_1(\text{grad}\mathbf{V}) + \frac{d\mathbf{A}_1}{dt} + (\text{grad}\mathbf{V})^t\mathbf{A}_1, \end{aligned} \right\} \tag{2}$$

in which d/dt is material time derivative, and \mathbf{V} is the velocity vector. This fact should be noticed that when $\alpha_1 = \alpha_2 = 0$, the fundamental equation for second-grade fluid reduces to that of viscous fluid. Employing the above assumption under boundary layer approximation, the equations that govern the flow are expressed as [27, 39]:

$$\frac{\partial}{\partial \dot{r}} ((\dot{r} + \dot{R}_c^*)\dot{v}) + \dot{R}_c^* \frac{\partial \dot{u}}{\partial \dot{s}} = 0, \tag{3}$$

$$\begin{aligned} \frac{\dot{u}^2}{\dot{r} + \dot{R}_c^*} &= \frac{1}{\dot{\rho}_{nf}} \frac{\partial P}{\partial \dot{r}}, \dot{v} \frac{\partial \dot{u}}{\partial \dot{r}} + \frac{\dot{R}_c^* \dot{u}}{\dot{r} + \dot{R}_c^*} \frac{\partial \dot{u}}{\partial \dot{s}} + \frac{\dot{u}\dot{v}}{\dot{r} + \dot{R}_c^*} \\ &= -\frac{1}{\dot{\rho}_{nf}} \frac{\dot{R}_c^*}{\dot{r} + \dot{R}_c^*} \frac{\partial P}{\partial \dot{s}} + v_{nf} \left(\frac{\partial^2 \dot{u}}{\partial \dot{r}^2} + \frac{1}{\dot{r} + \dot{R}_c^*} \frac{\partial \dot{u}}{\partial \dot{r}} - \frac{\dot{u}}{(\dot{r} + \dot{R}_c^*)^2} \right) \end{aligned} \tag{4}$$

$$+ \frac{\alpha_1}{\dot{\rho}_{nf}} \left(\begin{aligned} &\frac{2\dot{R}_c^*}{\dot{r} + \dot{R}_c^*} \frac{\partial^2 \dot{u}}{\partial \dot{r}^2} \frac{\partial \dot{u}}{\partial \dot{s}} - \frac{2\dot{R}_c^*}{(\dot{r} + \dot{R}_c^*)^2} \frac{\partial \dot{u}}{\partial \dot{r}} \frac{\partial \dot{u}}{\partial \dot{s}} + \frac{2}{\dot{r} + \dot{R}_c^*} \dot{v} \frac{\partial^2 \dot{u}}{\partial \dot{r}^2} \\ &- \frac{2}{(\dot{r} + \dot{R}_c^*)^2} \dot{v} \frac{\partial \dot{u}}{\partial \dot{r}} - \frac{4\dot{R}_c^*}{(\dot{r} + \dot{R}_c^*)^2} \dot{u} \frac{\partial^2 \dot{u}}{\partial \dot{r} \partial \dot{s}} - \frac{4\dot{u}}{(\dot{r} + \dot{R}_c^*)^2} \frac{\partial \dot{v}}{\partial \dot{r}} + \frac{2\dot{R}_c^*}{(\dot{r} + \dot{R}_c^*)^3} \dot{u} \frac{\partial \dot{u}}{\partial \dot{s}} \end{aligned} \right), \tag{5}$$

$$\begin{aligned} \dot{v} \frac{\partial \dot{T}}{\partial \dot{r}} + \frac{\dot{R}_c^* \dot{u}}{\dot{r} + \dot{R}_c^*} \frac{\partial \dot{T}}{\partial \dot{s}} &= \alpha_{nf} \left(\frac{\partial^2 \dot{T}}{\partial \dot{r}^2} + \frac{1}{\dot{r} + \dot{R}_c^*} \frac{\partial \dot{T}}{\partial \dot{r}} \right) \\ &- \frac{1}{\dot{\rho}_{nf}(\dot{r} + \dot{R}_c^*)} \frac{\partial}{\partial \dot{r}} (\dot{r} + \dot{R}_c^*) \dot{q}_r + \frac{\dot{\gamma}}{(\dot{\rho}C_p)_{nf}} (\dot{T} - \dot{T}_\infty). \end{aligned} \tag{6}$$

The associated constraints are as follows:

$$\left. \begin{aligned} \dot{u} &= a\dot{s}, \dot{v} = 0, \dot{T} = \dot{T}_w && \text{at } \dot{r} = 0, \\ \dot{u} \rightarrow 0, \frac{\partial \dot{u}}{\partial \dot{r}} \rightarrow 0, \dot{T} \rightarrow \dot{T}_\infty && \text{as } \dot{r} \rightarrow \infty. \end{aligned} \right\} \tag{7}$$

where \dot{v} and \dot{u} are velocities along \dot{r} and \dot{s} directions, respectively, for the curved sheet \dot{R}_c^* indicates its radius of curvature, \dot{T} stands for base fluid’s (second grade fluid) temperature, P for dimensionless pressure, \dot{q}_r for radiative heat flux, $\dot{\gamma}$ for rate of volumetric heat generation caused by heat source. Furthermore, $(\dot{\rho}C_p)_{nf}$ stands for volumetric heat

capacity of nanofluid $\hat{\mu}_{nf}$ for dynamic viscosity of nanofluid \hat{k}_{nf} for thermal conductivity and α_{nf} for thermal diffusivity and their mathematical expressions [12] are stated as

$$\left. \begin{aligned} \mu_{nf} &= \frac{\mu_f}{(1-\phi)^{2.5}}, \quad \alpha_{nf} = \frac{k_{nf}}{(\rho C_p)_{nf}}, \\ (\rho C_p)_{nf} &= (1-\phi)(\rho C_p)_f + \phi(\rho C_p)_{CNT}, \end{aligned} \right\} \quad (8)$$

$$\left. \begin{aligned} \frac{(\rho C_p)_{nf}}{(\rho C_p)_f} &= 1 - \left(1 - \frac{(\rho C_p)_{CNT}}{(\rho C_p)_f}\right)\phi, \\ \rho_{nf} &= (1-\phi)\rho_f + \phi\rho_{CNT}, \end{aligned} \right\} \quad (9)$$

$$\frac{k_{nf}}{k_f} = \frac{(1-\phi)(k_{CNT} - k_f) + 2\phi k_{CNT} \ln\left(\frac{k_{CNT} + k_f}{2k_f}\right)}{(1-\phi)(k_{CNT} - k_f) + 2\phi k_f \ln\left(\frac{k_{CNT} + k_f}{2k_f}\right)}, \quad (10)$$

where $\hat{\mu}_f$ stands for base fluid’s viscosity, ϕ for concentration of nanoparticles, α_{nf} for thermal diffusivity of nanofluid and (ρ_f, ρ_{CNT}) and (k_f, k_{CNT}) stands for density and thermal conductivity of base fluid (second grade fluid) and carbon nanotubes, respectively.

The term for radiative heat flux is estimated by Rooseland’s approximation [43] as:

$$\dot{q}_r = -\frac{4\hat{\sigma}^*}{3\hat{\alpha}_R} \frac{\partial \hat{T}^4}{\partial \hat{r}}, \quad (11)$$

where $\hat{\alpha}_R$ denotes the coefficient for Rooseland mean approximation and $\hat{\sigma}$ is Stefan–Boltzmann constant. Temperature variation is taken into account in such fashion that \hat{T}^4 can be expanded about \hat{T}_∞ using Taylor series expansion while omitting terms of higher order:

$$\hat{T}^4 \approx 4\hat{T}_\infty^3 \hat{T} - 3\hat{T}_\infty^4. \quad (12)$$

Now using Eq. (11) and Eq. (12) in Eq. (6) we get:

$$\begin{aligned} \hat{v} \frac{\partial \hat{T}}{\partial \hat{r}} + \frac{\hat{R}_c^* \hat{u}}{\hat{r} + \hat{R}_c^*} \frac{\partial \hat{T}}{\partial \hat{s}} &= \frac{\hat{k}_{nf}}{(\rho C_p)_{nf}} \left(1 + \frac{16\hat{\sigma}^* \hat{T}_\infty^3}{3\hat{\alpha}_R \hat{k}_f (\hat{k}_{nf}/\hat{k}_f)}\right) \\ &\left(\frac{\partial^2 \hat{T}}{\partial \hat{r}^2} + \frac{1}{\hat{r} + \hat{R}_c^*} \frac{\partial \hat{T}}{\partial \hat{r}}\right) + \frac{\hat{\gamma}}{(\rho C_p)_{nf}} (\hat{T} - \hat{T}_\infty). \end{aligned} \quad (13)$$

Taking $R_D = \frac{16\hat{\sigma}^* \hat{T}_\infty^3}{3\hat{\alpha}_R \hat{k}_f}$ as radiation parameter [44], Eq. (13) takes the form:

$$\begin{aligned} \hat{v} \frac{\partial \hat{T}}{\partial \hat{r}} + \frac{\hat{R}_c^* \hat{u}}{\hat{r} + \hat{R}_c^*} \frac{\partial \hat{T}}{\partial \hat{s}} &= \frac{v_f}{\lambda_3} \frac{1}{Pr} \frac{\hat{k}_{nf}}{\hat{k}_f} \left(1 + \frac{R_D}{(\hat{k}_{nf}/\hat{k}_f)}\right) \\ &\left(\frac{\partial^2 \hat{T}}{\partial \hat{r}^2} + \frac{1}{\hat{r} + \hat{R}_c^*} \frac{\partial \hat{T}}{\partial \hat{r}}\right) + \frac{\hat{\gamma}}{(\rho C_p)_{nf}} (\hat{T} - \hat{T}_\infty), \end{aligned} \quad (14)$$

where $Pr = \frac{v_f}{\hat{\alpha}_f}$, symbolizes Prandtl number. To simplify the governing equations, we engage the following similarity variables:

$$\left. \begin{aligned} \hat{u} &= \hat{\alpha} \hat{s} f'(\zeta), \quad \hat{v} = -\frac{\hat{R}_c^*}{\hat{r}_d + \hat{R}_c^*} \sqrt{\hat{\alpha} v_f} f(\zeta), \quad \zeta = \sqrt{\frac{\hat{\alpha}}{v_f}} \hat{r}, \\ P &= \rho \hat{\alpha}^2 \hat{s}^2 P(\zeta), \quad \hat{T} = \hat{T}_\infty + \frac{A \hat{\delta}}{l} \theta(\zeta), \quad \theta(\zeta) = \frac{\hat{T} - \hat{T}_\infty}{\hat{T}_w - \hat{T}_\infty}. \end{aligned} \right\} \quad (15)$$

With the help of Eq. (15), Eq. (3) is trivially satisfied and Eq. (4), Eq. (5) and Eq. (14) can be written as:

$$\begin{aligned} \frac{\partial P}{\partial \zeta} \frac{1}{\lambda_1} &= \frac{f'^2}{\zeta + \kappa}, \quad \frac{2\kappa}{\zeta + \kappa} \frac{P}{\lambda_1} - \frac{\kappa}{\zeta + \kappa} f f'' + \frac{\kappa}{\zeta + \kappa} f'^2 \\ &- \frac{\kappa}{(\zeta + \kappa)^2} f f' - \lambda_2 \left(f''' + \frac{1}{\zeta + \kappa} f'' - \frac{1}{(\zeta + \kappa)^2} f'\right) \end{aligned} \quad (16)$$

$$-\frac{\alpha_1}{\lambda_1} \left(-\frac{2\kappa}{(\zeta + \kappa)^2} (f f'' + 4f' f''') + \frac{2\kappa}{\zeta + \kappa} f' f'' + \frac{2\kappa}{(\zeta + \kappa)^3} (2f'' + 3f'^2) - \frac{4\kappa}{(\zeta + \kappa)^4} f f' \right) = 0, \quad (17)$$

$$\begin{aligned} &\left(1 + \frac{R_D}{(\hat{k}_{nf}/\hat{k}_f)}\right) \left(\theta'' + \frac{\theta'}{\zeta + \kappa}\right) \\ &- \frac{Pr}{(\hat{k}_{nf}/\hat{k}_f)} \left(\lambda_3 \frac{\kappa}{\zeta + \kappa} (f' \theta - f \theta') - \lambda_1 \theta\right) = 0, \end{aligned} \quad (18)$$

where $\kappa = \sqrt{\frac{\hat{\alpha}}{v_f}} \hat{R}_c^*$ symbolizes dimensionless radius of curvature $\alpha_1 = \frac{\hat{\alpha}_1 \hat{\alpha}}{\mu_f}$ and $\lambda_1 = \frac{\hat{\gamma}}{\hat{\alpha}(\rho C_p)_f}$ stands for heat generation parameter. If we set second-grade parameter $\alpha_1 = 0$ then the modeled governing equations will govern the rheological properties of Newtonian nanofluids (a limiting case). Further parameters λ_1, λ_2 and λ_3 are formulated as:

$$\left. \begin{aligned} \lambda_1 &= 1 - \phi + \phi \frac{\rho_{CNT}}{\rho_f}, \\ \lambda_2 &= \frac{1}{(1-\phi)^{2.5} \left(1 - \phi + \phi \frac{\rho_{CNT}}{\rho_f}\right)}, \\ \lambda_3 &= 1 - \left(1 - \frac{(\rho C_p)_{CNT}}{(\rho C_p)_f}\right)\phi. \end{aligned} \right\} \quad (19)$$

The utilization of Eq. (15) transforms Eq. (7) into dimensionless form as:

$$\left. \begin{aligned} f(0) = 0, f'(0) = 1, \theta(0) = 1, \\ f'(\infty) = 0, f''(\infty) = 0, \theta(\infty) = 0. \end{aligned} \right\} \tag{20}$$

Getting rid of pressure from Eq. (16) and Eq. (17) we get:

$$\begin{aligned} &\lambda_2 \left(f^{iv} + \frac{1}{(\zeta + \kappa)^3} f' - \frac{1}{(\zeta + \kappa)^2} f'' + \frac{2}{\zeta + \kappa} f''' \right) \\ &+ \frac{\kappa}{\zeta + \kappa} (ff''' - f'f'') \\ &+ \frac{\kappa}{(\zeta + \kappa)^2} (ff'' - f'^2) - \frac{\kappa}{(\zeta + \kappa)^3} ff' \\ &+ \frac{\alpha_1}{\lambda_1} \left(\frac{2\kappa}{\zeta + \kappa} (f'f^{iv} + f''f''') - \frac{10\kappa}{(\zeta + \kappa)^2} f'f''' - \frac{2\kappa}{(\zeta + \kappa)^2} ff^{iv} - \frac{8\kappa}{(\zeta + \kappa)^2} f'^2 \right. \\ &\left. + \frac{6\kappa}{(\zeta + \kappa)^3} ff''' + \frac{24\kappa}{(\zeta + \kappa)^3} f'f'' - \frac{16\kappa}{(\zeta + \kappa)^4} f'^2 - \frac{12\kappa}{(\zeta + \kappa)^4} ff'' + \frac{12\kappa}{(\zeta + \kappa)^5} ff' \right) = 0. \end{aligned} \tag{21}$$

Ultimately, pressure P can be obtained as follows:

$$P = \lambda_1 \frac{\zeta + \kappa}{2\kappa} \left(\begin{aligned} &\frac{\kappa}{\zeta + \kappa} ff''' - \frac{\kappa}{\zeta + \kappa} f'^2 + \frac{\kappa}{(\zeta + \kappa)^2} ff' + \lambda_2 \left(f''' + \frac{1}{\zeta + \kappa} f'' - \frac{1}{(\zeta + \kappa)^2} f' \right) \\ &- \frac{\alpha_1}{\lambda_1} \left(-\frac{2\kappa}{(\zeta + \kappa)^2} (ff''' + 4f'f'') + \frac{2\kappa}{\zeta + \kappa} f'f''' \right. \\ &\left. + \frac{2\kappa}{(\zeta + \kappa)^3} (2f'' + 3f'^2) - \frac{4\kappa}{(\zeta + \kappa)^4} ff' \right) \end{aligned} \right). \tag{22}$$

In δ -direction, the skin-friction coefficient (C_f) as well as local Nusselt number (Nu_δ) are defined as:

$$C_f = \frac{\tau_{\delta s}}{\rho_f u_w^2}, \quad Nu_\delta = \frac{(s_d \dot{q}_w)/k_f}{(\dot{T}_w - \dot{T}_\infty)} \tag{23}$$

where u_w is velocity in δ -direction, $\tau_{\delta s}$ and \dot{q}_w describes shear stress as well as heat flux at curved stretchable surface in δ -direction respectively as follows:

$$\left. \begin{aligned} \tau_{\delta s} &= \frac{1}{(1-\phi)^{2.5}} \mu_{nf} \left(\frac{\partial \dot{u}}{\partial r} - \frac{\dot{u}}{r+\dot{R}} + \frac{2\alpha_1}{\mu_{nf}} \left(\frac{\dot{v}}{r+\dot{R}} \frac{\partial \dot{u}}{\partial r} + \frac{\dot{R}}{r+\dot{R}} \frac{\partial \dot{u}}{\partial r} \frac{\partial \dot{u}}{\partial s} - \frac{2\dot{u}\dot{v}}{(r+\dot{R})^2} - \frac{2\dot{R}\dot{u}}{(r+\dot{R})^2} \frac{\partial \dot{u}}{\partial r} \right) \right) \Big|_{r=0}, \\ \dot{q}_w &= -k_{nf} \left(1 + \frac{16\sigma^* \dot{T}_\infty^3}{3\alpha_R k_f (k_{nf}/k_f)} \right) \frac{\partial \dot{T}}{\partial r} \Big|_{r=0}. \end{aligned} \right\} \tag{24}$$

Employing Eq. (15) in Eq. (23) and Eq. (24), we get expressions for skin-friction coefficient as well as local Nusselt number as:

$$\left. \begin{aligned} Re_\delta^{1/2} C_f &= \frac{1}{(1-\phi)^{2.5}} 2 \left(f''(0) - \frac{f'(0)}{\kappa} + \alpha_1 \left(-2 \frac{f'(0)^2}{\kappa} + f'(0) f''(0) \right) \right), \\ Re_\delta^{-1/2} Nu_\delta &= -\frac{k_{nf}}{k_f} \left(1 + \frac{R_D}{(k_{nf}/k_f)} \right) \theta'(0), \end{aligned} \right\} \tag{25}$$

where $Re_\delta = \frac{a\delta^2}{\nu_f}$ expresses local Reynolds number.

Numerical solution and discussion

The assessment of exact solution for the resultant system of nonlinear Eqs. (16), (18) and (21) together with boundary conditions (20) is a tedious task. A well systematic technique, namely shooting method is engaged using

software MATHEMATICA to get the numerical solution. Under the aegis of this approach, a boundary value problem (BVP) is transformed into an initial value problem (IVP) with first-order differential equations with a minimal number of lacking initial constraints. These lacking initial constraints are selected in such a way that they must satisfy the asymptotic boundary constraints. Table 1 along with Eqs. (8 – 10) is utilized to calculate numerical values of parameters formulated in Eq. (19), which are involved

in evaluating the exact solution for derived nonlinear systems of equations. The pressure effects can be calculated using Eq. (22). Table 2 is generated to assess the effectiveness and accuracy of the numerical technique employed in

Table 1 Thermophysical characteristics of carbon nanotubes (SWCNTs and MWCNTs) are tabulated as:

	ρ/Kgm^{-3}	$C_p/\text{Jkg}^{-1}\text{K}^{-1}$	$k/\text{Wm}^{-1}\text{K}^{-1}$
SWCNTs	2600	425	6600
MWCNTs	1600	796	3300

Table 2 Error analysis of the values of $-\text{Re}_s^{1/2} C_f$ to address the validity of numerical method with $R_D = \lambda_1 = \alpha_1 = 0$

ϕ	κ	Nagaraja et al. [45]	Current study		Percentage relative
			SWCNTs	MWCNTs	Absolute difference
0.0	5	1.15764	1.15763	1.15763	0.000864%
	10	1.07349	1.07349	1.07349	0%
	30	1.02352	1.02353	1.02353	0.000977%
	50	1.01407	1.01405	1.01405	0.001972%

this study. This table guarantees the validity of employed numerical technique by showcasing that our outcomes using shooting method aligns closely with results in existing literature obtained by Runge–Kutta–Fehlberg fourth–fifth-order method. Table 3 serves to present a comprehensive comparison between our results and the findings in existing literature, which shows an excellent agreement. After achieving the solution, this section is compiled to explore the effects of numerous parameters including dimensionless curvature (κ), solid volume fraction of CNTs (ϕ), heat generation parameter (λ_1), radiation parameter (R_D) and Prandtl number (Pr) on focused physical quantities, i.e., velocity $f'(\zeta)$ and temperature $\theta(\zeta)$ of fluid. The effect of dimensionless curvature (κ) on fluid's velocity $f'(\zeta)$ is unveiled in Fig. 2. It can be seen that an upsurge in values of dimensionless curvature (κ) causes a decline in fluid's velocity $f'(\zeta)$. This is due to the fact that value of κ determines the flow regime in curved surface. For low values of κ ($\kappa \ll 1$), the flow is considered to be in the "low-curvature" regime, where the effects of curvature are negligible. However, for high values of κ ($\kappa \gg 1$), the flow is in the "high-curvature" regime, where curvature has a significant influence on the flow behavior. The influence of solid volume fraction (ϕ) of CNTs on velocity profile $f'(\zeta)$ of nanofluid is unveiled in Fig. 3. A certain inflation has been noticed as the solid volume fraction (ϕ) of CNTs is increased. As the solid volume fraction (ϕ) of CNTs in the fluid increases, the number of

collisions between the nanotubes and the fluid molecules also increases. These collisions cause the nanoparticles to move around in a random manner, which is known as the Brownian motion effect. This random movement of the nanoparticles creates a more chaotic environment for the fluid molecules, thereby enhancing their velocity. Moreover it has been noted that SWCNTs have slightly less velocity as compared to MWCNTs due to greater density values of MWCNTs. Figure 4 portrays the influence of second-grade fluid parameter (α_1) over fluid's velocity $f'(\zeta)$. As the second-grade fluid parameter gets amplified, the velocity rises. This is because the added elasticity of the fluid can enhance its ability to resist deformation under shear. The fluid's higher elasticity allows it to absorb and store more energy, resulting in greater momentum transfer and increased velocity. Figure 5 elucidates the impact of dimensionless curvature (κ) on temperature profile $\theta(\zeta)$. Physically larger values of (κ) corresponds to reduction in viscous force (i.e., decay in kinematic velocity of fluid). Decay in kinematic viscosity of fluid corresponds to lower heat transfer. Hence, a declination in temperature profile $\theta(\zeta)$ is certain. Figure 6 unveils the action of solid volume fraction (ϕ) of CNTs on temperature profile $\theta(\zeta)$. Carbon nanotubes (both single and multiple-walled) have relatively greater thermal conductivity and lesser specific heat than base fluid (second grade fluid). So increasing their volume (ϕ) in nanofluid will cause a rise in $\theta(\zeta)$. Moreover as the volume fraction (ϕ) of carbon nanotubes in the fluid increases, the movement of fluid molecules becomes more restricted and the frictional forces between the fluid and the solid particles increase. This increase in frictional forces results in an increase in heat generation, which raises the temperature of the fluid. Additionally, carbon nanotubes themselves can absorb heat and transfer it to the surrounding fluid, which can further increase the temperature. Action on temperature profile $\theta(\zeta)$ by heat generation parameter (λ_1) elucidates Fig. 7. The heat generation parameter (λ_1) is a measure of the amount of energy being generated per unit volume of the fluid. As the heat generation parameter (λ_1) increases, the amount of energy being generated per unit volume of the fluid also increases.

Table 3 Comparative analysis of the values of $-\text{Re}_s^{1/2} C_f$ for distinct numerics of κ and ϕ , with $R_D = \lambda_1 = \alpha_1 = 0$

ϕ	κ	Abbas et al. [46]	Saba et al. [40]		Current study	
			SWCNTs	MWCNTs	SWCNTs	MWCNTs
0.0	5	1.15763	1.15763	1.15763	1.15763	1.15763
	10	1.07349	1.07349	1.07349	1.07349	1.07349
	50	1.01405	1.01405	1.01405	1.01405	1.01405
	1000	1.00079	1.00079	1.00079	1.00079	1.00079
0.1	5	–	1.43781	1.38677	1.43707	1.38669
	10	–	1.32577	1.27251	1.32569	1.27247
	50	–	1.27579	1.22190	1.27549	1.22186

Table 4 Numerical data for local Nusselt number and skin friction coefficient for various parameters

ϕ	α_1	λ_1	R_D	SWCNTs				MWCNTs			
				$Re_s^{1/2} C_f$		$Re_s^{-1/2} Nu_s$		$Re_s^{1/2} C_f$		$Re_s^{-1/2} Nu_s$	
0.0	0.3	0.1	0.1	-3.09927		-1.48942		-3.09927		-1.52424	
0.3				-3.56770	↓	-1.48227	↑	-3.27669	↓	-1.51863	↑
0.5				-3.97289	↓	-1.44833	↑	-3.64933	↓	-1.48731	↑
0.7				-5.19836		-1.37694		-4.98352		-1.41830	
0.1	0.3	0.1	0.1	-3.75080		-1.57626		-3.67442		-1.59220	
	0.4			-3.89063	↓	-1.59300	↓	-3.80818	↓	-1.60926	↓
	0.5			-4.03592	↓	-1.60758	↓	-3.94744	↓	-1.62415	↓
	0.6			-4.18728		-1.62017		-4.09278		-1.63704	
0.1	0.3	0.1	0.1	-3.26908		-1.49443		-3.14391		-1.51198	
		0.2		-3.26908	-	-1.39034	↑	-3.14391	-	-1.41178	↑
		0.3		-3.26908	-	-1.25988	↑	-3.14391	-	-1.29045	↑
		0.4		-3.26908		-1.16865		-3.14391		-1.21177	
0.1	0.3	0.1	0.1	-3.26908		-1.49443		-3.14391		-1.51198	
		0.3		-3.26908	-	-1.59302	↓	-3.14391	-	-1.61358	↓
		0.5		-3.26908	-	-1.68015	↓	-3.14391	-	-1.70362	↓
		0.7		-3.26908		-1.75847		-3.14391		-1.78468	

This leads to an increase in the amount of heat energy transferred to the fluid, causing the temperature $\theta(\zeta)$ of the fluid to rise. Figure 8 depicts the sway of radiation parameter (R_D) on temperature of fluid $\theta(\zeta)$. As predicted, the fluid’s temperature amplifies quite significantly as an upsurge in (R_D). The radiation parameter (R_D) comprises mean absorption coefficient which reduces as increase in (R_D) consequently the heat transfer rate seems increases at every point away from sheet. Hence, an increase in fluid’s temperature is certain. When using slurry mixtures as base fluid, it is worth noting that these are examined by taking the value of Prandtl number as 5.83, which is lower as compared to water and other common base fluids. Prandtl number is the ratio of momentum diffusivity to thermal diffusivity that’s why its larger values decline the temperature distribution. The effect of dimensionless curvature (κ) on pressure profile $P(\zeta)$ is explained in Fig. 9. One can notice that an increment in value of (κ) causes an upsurge in pressure inside the boundary layer. However, pressure approaches to zero far away from the boundary. This is because as we move far from boundary the stream lines of fluid flow conduct the same manner as for the case of flat stretching surface. Moreover, Fig 10 guarantees that pressure variations can be neglected throughout the flow for the case ($\kappa = 1000$), i.e., a flat stretching sheet, while it cannot be neglected for curved surfaces.

Figure 11 shows the impact of dimensionless curvature over skin friction coefficient (C_f). An amplification in dimensionless curvature (κ) leads to a rise in skin friction coefficient (C_f) in a flow over a curved stretching surface due to the increased surface area of the curved surface. As the dimensionless curvature (κ) of the surface rises,

the surface area also gets broadened, which can lead to a higher skin friction coefficient (C_f). This is due to the fact that the fluid molecules in contact with the surface experience a higher shear stress as the dimensionless curvature (κ) rises, resulting in a boost in skin friction coefficient (C_f). Figure 12 portrays the influence of dimensionless curvature (κ) over local Nusselt number (Nu_s). As the dimensionless curvature of the surface rises (κ), the surface area also expands, which can lead to a rise in the convective heat transfer coefficient and, subsequently, an increment in the local Nusselt number (Nu_s). Additionally, the boundary layer thickness drops as the dimensionless curvature (κ) of the surface rises, resulting in an increment in heat transfer rate at the surface, which can also contribute to a rise in the local Nusselt number (Nu_s). Table 4 displays how several factors such as solid volume fraction of carbon nanotubes (ϕ), radiation parameter (R_D) and internal heat generation parameter (λ_1) affects skin-friction coefficient (C_f) and local Nusselt number (Nu_s) defined in Eq. (25). An increment in solid volume fraction of carbon nanotubes (ϕ) reduces the skin friction coefficient (C_f) due to the unique properties of carbon nanotubes. These properties, such as their high aspect ratio and excellent thermal conductivity enhances the transfer of heat and momentum in the fluid, which leads to a reduction in skin friction coefficient (C_f). When the second-grade fluid parameter (α_1) is higher, fluid’s viscosity tends to decrease with increasing shear rate. This decrease in viscosity with shear rate is known as shear-thinning behavior. The shear-thinning behavior of the second-grade fluid leads to the reduction in the effective viscosity near the surface, resulting in decline of skin friction coefficient (C_f). Furthermore

thermal radiation (R_D) and internal heat generation (λ_1) do not change the value of the local skin friction coefficient (C_f) because they do not directly affect the shear stress at the surface. Skin friction coefficient is the ratio of shear stress to the dynamic pressure of the fluid and is based solely on the fluid properties and flow conditions at the surface. Thermal radiation (R_D) and internal heat generation (λ_1) are related to the energy balance of the fluid, but they do not directly influence the fluid flow behavior at the surface. Therefore, they do not affect the skin friction coefficient (C_f).

Carbon nanotubes have enhanced thermal conductivity, which can amplify the transfer of heat between the fluid and the surface. As the solid volume fraction of carbon nanotubes (ϕ) strengthens, so does the thermal conductivity of the nanofluid, which leads to an advancement in the local Nusselt number (Nu_s). Increment in second-grade fluid parameter (α_1) leads to formation of thicker boundary layer near the solid surface. The thicker boundary layer acts as a barrier to heat transfer, reducing the convective heat transfer coefficient. As a result, the convective heat transfer decreases, resulting in lower local Nusselt number (Nu_s). The Nusselt number (Nu_s) is a dimensionless parameter that relates the convective heat transfer coefficient to the thermal conductivity of the fluid and the characteristic length of the surface. It has been perceived that rate of heat flux raises as an upsurge in radiation parameter (R_D) contains mean absorption coefficient which generates as rise in (R_D). For this reason, the heat transfer rate seems maximizing at every point away from sheet. So, the local Nusselt number gets amplified as a rise in radiation parameter (R_D). Moreover, an increment in heat generation parameter (λ_1) causes a reduction in local Nusselt number (Nu).

Conclusions

This investigation scrutinizes heat transmission through a radiative flow of boundary layer nature incorporating heat generation of second-grade nanofluid (slurry mixture) containing carbon nanotubes (SWCNTs and MWCNTs) overtop a curved extending surface. Main highlights are:

- The velocity profile $f'(\zeta)$ gets amplified as an upsurge in solid volume fraction (ϕ) and second-grade parameter (α_1) and reduces as an increment in dimensionless curvature (κ).
- The temperature $\theta(\zeta)$ of the fluid rises due to amplification of heat generation parameter (λ_1), radiation parameter (R_D) and solid volume fraction (ϕ) of carbon nanotubes, while an opposite trend is noticed for the upsurge in dimensionless curvature (κ).

- The skin friction coefficient (C_f) drops due to an increment in solid volume fraction (ϕ) and it gets amplified due to a rise in dimensionless curvature (κ) and it remains invariant for upsurge in radiation parameter (R_D) and internal heat generation (λ_1).
- Local Nusselt (Nu_s) number rises as an upsurge in values of solid volume fraction (ϕ), dimensionless curvature (κ) and internal heat generation (λ_1), while it diminishes as a rise in radiation parameter (R_D).

Acknowledgment The authors extend their appreciation to the research unit at King Khalid University for funding this work through Project number 495 and the authors acknowledge the Research Center for Advanced Materials Science (RCAMS) at King Khalid University, Saudi Arabia for their valuable technical support.

References

1. Choi SUS. Enhancing thermal conductivity of fluids with nanoparticles. *Dev Appl Non Newton Flows*. 1995;232:99–105.
2. Kim J, Kang YT, Choi CK. Analysis of convective instability and heat transfer characteristics of nanofluids. *Phys Fluids*. 2004;16:2395–401.
3. Buongiorno J. Convective transport in nanofluids. *J Heat Transf*. 2006;128:240–50.
4. Tiwari RK, Das MK. Heat transfer augmentation in a two-sided lid-driven differentially heated square cavity utilizing nanofluids. *Int J Heat Mass Transf*. 2007;50:2002–18.
5. Khan WA, Pop I. Boundary-layer flow of a nanofluid past a stretching sheet. *Int J Heat Mass Transf*. 2010;53:2477–83.
6. Kuznetsov AV, Nield DA. Natural convective boundary-layer flow of a nanofluid past a vertical plate. *Int J Therm Sci*. 2010;49:243–7.
7. Raza J, Rohni AM, Omar Z. Numerical investigation of copper-water (Cu-Water) nanofluid with different shapes of nanoparticles in a channel with stretching wall: slip effects. *Math Comput Appl*. 2016;21:43.
8. Hayat T, Rashid M, Alsaedi A. MHD convective flow of magnetite-Fe₃O₄ nanoparticles by curved stretching sheet. *Results Phys*. 2017;7:3107–15.
9. Saif RS, Muhammad T, Sadia H, Ellahi R. Hydromagnetic flow of Jeffrey nanofluid due to a curved stretching surface. *Phys A: Stat Mech*. 2020;551:0378–4371.
10. Saif RS, Hashim M, Zaman M. Ayaz. Thermally stratified flow of hybrid nanofluids with radiative heat transport and slip mechanism: multiple solutions. *Commun Theor Phys*. 2022;74: 015801.
11. Maxwell JC. *A Treatise on Electricity and Magnetism*. 3rd ed. Oxford, UK: Oxford University Press; 1904.
12. Xue QZ. Model for thermal conductivity of carbon nanotube-based composites. *Phys B Condens Matter*. 2005;368:302–7.
13. Khan U, Ahmed N, Mohyud-Din ST. Stoke's first problem for carbon nanotubes suspended nanofluid flow under the effect of slip boundary condition. *J Nanofluids*. 2016;5(2):239–44.
14. Hayat T, Khalid H, Waqas M, Alsaedi A. Numerical simulation for radiative flow of nanoliquid by rotating disk with carbon nanotubes and partial slip. *Comput Methods Appl Mech Eng*. 2018;341:397–408.

15. Wakif A, Boulahia Z, Sehaqui R. A semi-analytical analysis of electro-thermo-hydrodynamic stability in dielectric nanofluids using Buongiorno's mathematical model together with more realistic boundary conditions. *Results Phys.* 2018;9:1438–54.
16. Khan MI, Shah F, Hayat T, Alsaedi A. Transportation of CNTs based nanomaterial flow confined between two coaxially rotating disks with entropy generation. *Phys A: Stat Mech.* 2019;527: 121154.
17. Acharya N, Bag R, Kundu PK. On the mixed convective carbon nanotube flow over a convectively heated curved surface. *Heat Transf Res.* 2020;49:1713–35.
18. Al-Hanaya AM, Sajid F, Abbas N, Nadeem S. Effect of SWCNT and MWCNT on the flow of micropolar hybrid nanofluid over a curved stretching surface with induced magnetic field. *Sci Rep.* 2020;10:8488.
19. Ahmad S, Nadeem S, Muhammad N, Khan MN. Cattaneo-Christov heat flux model for stagnation point flow of micropolar nanofluid toward a nonlinear stretching surface with slip effects. *J Therm Anal Calorim.* 2021;143:1187–99.
20. Bhatti MM, Ellahi R, Doranehgard MH. Numerical study on the hybrid nanofluid (Co3O4-Go/H2O) flow over a circular elastic surface with non-Darcy medium: Application in solar energy. *J Mol Liq.* 2022;361: 119655.
21. Bhatti MM, Öztop HF, Ellahi R. Study of the magnetized hybrid nanofluid flow through a flat elastic surface with applications in solar energy. *Materials.* 2022;15:7507.
22. Bhatti MM, Ellahi R. Numerical investigation of non-Darcian nanofluid flow across a stretchy elastic medium with velocity and thermal slips. *Numer Heat Transfer.* 2023;83(5):323–43.
23. Hayat T, Sajid M. Analytic solution for axisymmetric flow and heat transfer of a second-grade fluid past a stretching sheet. *Int J Heat Mass Transf.* 2007;50(1):75–84.
24. Saif RS, Hayat T, Ellahi R, Muhammad T, Alsaedi A. Stagnation-point flow of second grade nanofluid towards a nonlinear stretching surface with variable thickness. *Results Phys.* 2017;7:2821–30.
25. Wakif A. A novel numerical procedure for simulating steady MHD convective flows of radiative Casson fluids over a horizontal stretching sheet with irregular geometry under the combined influence of temperature-dependent viscosity and thermal conductivity. *Math Problem Eng.* 2020. <https://doi.org/10.1155/2020/1675350>.
26. Hayat T, Ahmad S, Khan MI, Alsaedi A. Non-Darcy Forchheimer flow of ferromagnetic second-grade fluid. *Results Phys.* 2017;7:3419–24.
27. Jamshed W, Nisar KS, Gowda RJP, Kumar RN, Prasannakumara BC. Radiative heat transfer of second grade nanofluid flow past a porous flat surface: a single-phase mathematical model. *Phys Scr.* 2021;96(6): 064006.
28. Gowda RJP, Baskonus HM, Kumar RN, Prasannakumara BC, Prakasha DG. Computational investigation of Stefan blowing effect on flow of second-grade fluid over a curved stretching sheet. *Int J Appl Comput Math.* 2021;7(3):109.
29. Khan SU, Tlili I, Waqas H, Imran M. Effects of nonlinear thermal radiation and activation energy on modified second-grade nanofluid with Cattaneo-Christov expressions. *J Therm Anal Calorim.* 2021;143:1175–86.
30. Khan AA, Khan MN, Ahsan N, Khan MI, Muhammad T, Rehman A. Heat and mass transfer features of transient second-grade fluid flow through an exponentially stretching surface. *Pramana-J Phys.* 2022;96:58.
31. Abbas SZ, Waqas M, Thaljaoui A, Zubair M, Riahi A, Chu YM, Khan WA. Modeling and analysis of unsteady second-grade nanofluid flow subject to mixed convection and thermal radiation. *Soft Comput.* 2022;26:1033–42.
32. Noureddine E, Cherlacola SR, Ahmed A, Sayed E, Taseer M, Wakif A. A passive control approach for simulating thermally enhanced Jeffery nanofluid flows nearby a sucked impermeable surface subjected to buoyancy and Lorentz forces. *Case Stud Thermal Eng.* 2023;47: 103106.
33. Sakiadis BC. Boundary-layer behavior on continuous solid surfaces: II. The boundary layer on a continuous flat surface. *AIChE J.* 1961;7:221–5.
34. Crane LJ. Flow past a stretching plate. *J Appl Math Phys (ZAMP).* 1970;21:645–7.
35. Sajid M, Ali N, Javed T, Abbas Z. Stretching a curved surface in a viscous fluid. *Chin Phys Lett.* 2010;27: 024703.
36. Hayat T, Saif RS, Ellahi R, Muhammad T, Ahmad B. Numerical study for Darcy-Forchheimer flow due to a curved stretching surface with Cattaneo-Christov heat flux and homogeneous-heterogeneous reactions. *Results Phys.* 2017;7:2886–92.
37. Hayat T, Saif RS, Ellahi R, Muhammad T, Ahmad B. Numerical study of boundary-layer flow due to a nonlinear curved stretching sheet with convective heat and mass conditions. *Results Phys.* 2017;7:2601–6.
38. Reddy JVR, Sugunamma V, Sandeep N. Effect of frictional heating on radiative ferrofluid flow over a slendering stretching sheet with aligned magnetic field. *Eur Phys J Plus.* 2017;132:7.
39. Hayat T, Saif RS, Ellahi R, Alsaedi A, Muhammad T. Homogeneous-heterogeneous reactions in MHD flow of micropolar fluid by a curved stretching surface. *J Mol Liq.* 2017;240:209–20.
40. Saba F, Ahmed N, Hussain S, Khan U, Mohyud-Din ST, Darus M. Thermal analysis of nanofluid flow over a curved stretching surface suspended by carbon nanotubes with internal heat generation. *Appl Sci.* 2018;8:395.
41. Saif RS, Muhammad T, Sadia H, Ellahi R. Hydromagnetic flow of Jeffrey nanofluid due to a curved stretching surface. *Phys A: Stat Mech Appl.* 2020;551:0378–4371.
42. Raza R, Mabood F, Naz R, Abdelsalam SI. Thermal transport of radiative Williamson fluid over stretchable curved surface. *Therm Sci Eng Prog.* 2021;23:2451–9049.
43. Rosseland S. *Astrophysik Und Atom-Theoretische Grundlagen.* Berlin, Germany: Springer; 1931.
44. Magyari E, Pantokratoras A. Note on the effect of thermal radiation in the linearized Rosseland approximation on the heat transfer characteristics of various boundary layer flows. *Int Commun Heat Mass Transf.* 2011;38:554–6.
45. Nagaraja B, Gireesha BJ. Exponential space-dependent heat generation impact on MHD convective flow of Casson uid over a curved stretching sheet with chemical reaction. *J Therm Anal Calorim.* 2021;143:4071–9.
46. Abbas Z, Naveed M, Sajid M. Heat transfer analysis for stretching flow over a curved surface with magnetic field. *J Eng Thermophys.* 2013;22:337–45.

Publisher's Note Springer Nature remains neutral with regard to jurisdictional claims in published maps and institutional affiliations.

Springer Nature or its licensor (e.g. a society or other partner) holds exclusive rights to this article under a publishing agreement with the author(s) or other rightsholder(s); author self-archiving of the accepted manuscript version of this article is solely governed by the terms of such publishing agreement and applicable law.